Journal of Solid State Chemistry 322 (2023) 123937

Contents lists available at ScienceDirect

Journal of Solid State Chemistry

journal homepage: www.elsevier.com/locate/jssc

Composition-, temperature- and pressure-induced transitions between high-pressure stabilized perovskite phases of the (1-*x*)$BiFe_{0.5}Sc_{0.5}O_3$ - *x*$LaFe_{0.5}Sc_{0.5}O_3$ series

A.N. Salak [a,*], J.P. Cardoso [a], D.D. Khalyavin [b,**], A. Barbier [c], P. Fertey [d], S.M. Mikhalev [e], N.M. Olekhnovich [f], A.V. Pushkarev [f], Yu V. Radyush [f], A. Stanulis [g], R. Ramanauskas [g]

[a] Department of Materials and Ceramic Engineering, CICECO – Aveiro Institute of Materials, University of Aveiro, Aveiro, 3810-193, Portugal
[b] ISIS Facility, Rutherford Appleton Laboratory, Chilton, Didcot, OX11 0QX, UK
[c] SPEC, CEA, CNRS, Université Paris-Saclay, CEA-Saclay, Gif-sur-Yvette Cedex, 91191, France
[d] Synchrotron SOLEIL, L'Orme des Merisiers, St Aubin BP48, Gif sur Yvette Cedex, 91192, France
[e] Department of Mechanical Engineering, TEMA – Centre for Mechanical Technology and Automation, University of Aveiro, Aveiro, 3810-193, Portugal
[f] Scientific-Practical Materials Research Centre of NAS of Belarus, Minsk, 220072, Belarus
[g] Department of Chemical Engineering and Technology, Center for Physical Sciences and Technology, Vilnius, LT-10257, Lithuania

ARTICLE INFO

Keywords:
High-pressure synthesis
Metastable perovskite phase
Incommensurate modulation

ABSTRACT

Crystal structures of the high-pressure synthesized perovskite phases of the (1-*x*)$BiFe_{0.5}Sc_{0.5}O_3$-*x*$LaFe_{0.5}Sc_{0.5}O_3$ ($0 = x \leq 1$) system and their temperature and pressure behaviours were studied using laboratory and synchrotron X-ray diffractions as well as neutron diffraction. At room temperature, the as-prepared phases with $x \leq 0.05$ have an antipolar structure with the *Pnma* symmetry and with the $\sqrt{2}a_p \times 4a_p \times 2\sqrt{2}a_p$ superstructure (where a_p is the pseudocubic perovskite unit-cell parameter). An incommensurately modulated phase with the *Imma*(00γ)*s*00 superspace group is observed for $0.10 = x \leq 0.33$, while a non-polar *Pnma* phase ($\sqrt{2}a_p \times 2a_p \times \sqrt{2}a_p$) is stable when $x \geq 0.34$. The antipolar *Pnma* phase in the as-prepared samples with composition corresponding to $x = 0$ transforms into the polar *Ima*2 one *via irreversible* annealing-caused transformation accompanied by a formation of a high-temperature intermediate polar *R*3*c* polymorph, while the antipolar *Pnma* phase in samples with $x = 0.05$ is stable until the decomposition temperature. In the solid solutions with $0.10 = x \leq 0.33$, increasing temperature was found to result in a *reversible* transformation of the *Imma*(00γ)s00 phase into a non-polar *Pnma* one. The transition temperature decreases with increasing *x*. A hydrostatic pressure of few GPa was also shown to induce a *reversible Imma*(00γ)s00 → *Pnma* transformation.

1. Introduction

Bismuth ferrite, one of few type-I multiferroics, is a unique model object for fundamental studies on structure-dependent magnetic and polar orderings and their interrelations [1]. In addition to the evident possibilities of practical applications of $BiFeO_3$ as multiferroic material in magnetic field sensors, electrically switchable magnets, magnetic memory and spin electronic devices [2], new areas of applications such as photovoltaics, photocatalysis, and electric energy storage [3–5] were recently demonstrated. However, in the overwhelming majority of cases, practical application of $BiFeO_3$ requires chemical modifications, which are generally needed to overcome the drawbacks intrinsic to this compound, namely high values of both the Néel temperature and the Curie point, the modulated spin ordering that averages the net magnetization to zero and very high electroconductivity [1,6,7].

Many materials were obtained by means of chemical modification of bismuth ferrite. They mostly result from atomic substitutions in the bismuth site (see e.g. Refs. [8–11], and references therein). More than 10 at.% replacements of iron, as a rule, are impossible to achieve using conventional synthesis techniques and require high-pressure synthesis [12–19]. Therefore, Bi(*B*,Fe)O_3 compositions are much less studied than (*A*,Bi)FeO_3.

We previously reported a high-pressure synthesized $BiFe_{0.5}Sc_{0.5}O_3$ ceramics and described crystal structures of the perovskite phases

* Corresponding author.
** Corresponding author.
E-mail addresses: salak@ua.pt (A.N. Salak), dmitry.khalyavin@stfc.ac.uk (D.D. Khalyavin).

https://doi.org/10.1016/j.jssc.2023.123937
Received 15 January 2023; Received in revised form 21 February 2023; Accepted 23 February 2023
Available online 25 February 2023

detected at different stages of annealing [20]. As-prepared (non-annealed) samples were found to have antipolar orthorhombic *Pnma* symmetry with the $\sqrt{2}a_p \times 4a_p \times 2\sqrt{2}a_p$ superstructure resulted from displacements of Bi^{3+} and unusual "+ + − − + + − −" octahedral tilting about the orthorhombic *b* axis (pseudocubic $[010]_p$). We showed that annealing induces transformation of the antipolar phase of $BiFe_{0.5}Sc_{0.5}O_3$ into a polar *R*3*c* phase, which is turned into a polar *Ima*2 phase ($2a_p \times \sqrt{2}a_p \times \sqrt{2}a_p$) on cooling. The *Ima*2 phase represents an original type of a canted ferroelectric structure where Bi^{3+} cations exhibit both polar and antipolar displacements along the orthogonal $[110]_p$ and $[1\bar{1}0]_p$ pseudocubic directions, respectively. The crossover *Pnma* → *R*3*c* → *Ima*2 is irreversible at atmospheric pressure. Direct return *Ima*2 → *Pnma* transition (irreversible as well) is possible at room temperature under high pressure only [20].

In this paper, we report on high-pressure synthesis and crystal structure characterization of the compositions derived from $BiFe_{0.5}Sc_{0.5}O_3$, in which bismuth is substituted by lanthanum over the entire range ($Bi_{1-x}La_xFe_{0.5}Sc_{0.5}O_3$, hereinafter BL*x*FSO, $0 = x \leq 1$). Bismuth-to-lanthanum substitution in $BiFeO_3$ is known to lead to series of structural phase transformations [9,11,21]. New perovskite phases and phase transitions (both reversible and irreversible) were anticipated in BL*x*FSO as well. Besides, such a substitution is one of the simplest ways to decrease to ferroelectric transition temperature [22] and reduce high conductivity of $BiFe_{0.5}Sc_{0.5}O_3$ [23].

Actually, the solid solution series prepared and studied in this work is a section of the quasi-quaternary $BiFeO_3$-$BiScO_3$-$LaFeO_3$-$LaScO_3$ system ($Bi_{1-x}La_xFe_ySc_{1-y}O_3$, $0 = x \leq 1$ and $0 = y \leq 1$) at the 1:1 Fe/Sc ratio (Scheme 1).

Some particular BL*x*FSO compositions were characterized earlier. In particular, the composition with $x = 0.20$ was found to crystalize in perovskite structure with incommensurate modulation that is described using the *Imma*(00γ)*s*00 superspace group [24]. We also showed that the compositional crossover from the incommensurately modulated antipolar *Imma*(00γ)*s*00 phase to the non-polar *Pnma* phase in BL*x*FSO at room temperature occurs between $x = 0.33$ and 0.34 with no range of phase coexistence [22].

2. Experimental procedure

The BL*x*FSO ceramics of the entire compositional range ($0 = x \leq 1$) were synthesized under high pressure from the ball-milled stoichiometric mixtures of the high-purity oxides and from the precursors produced *via* a sol-gel combustion route using nitrates of the respective metals. A sol-gel method for the precursor preparation was used only to ensure precise chemical composition of the samples in the narrow compositional range of $0.30 = x \leq 0.35$ in which the BL*x*FSO solid solutions were studied with a step of $\Delta x = 0.01$. Details of the precursor preparation and the high-pressure synthesis can be found in Refs. [20,22]. The single-phase perovskite ceramics with compositions in the range of $x \geq 0.8$ were also prepared using the conventional ceramic route.

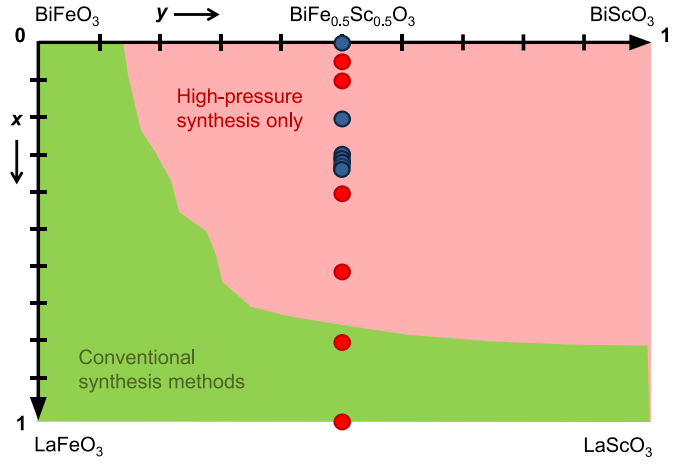

Scheme 1. The *x*-*y* range of the $Bi_{1-x}La_xFe_ySc_{1-y}O_3$ solid solutions with the tentative compositional fields in which perovskite phases can be obtained using the conventional solid-state synthesis or the high-pressure synthesis only. The blue circles indicate the previously reported BL*x*FSO compositions [20,22,24,25], red solid circles correspond to the compositions studied in this work.

The microstructure of the ceramics was studied using a Hitachi SU-70 scanning electron microscope (SEM) operated at 25 kV.

An X-ray diffraction (XRD) study of the obtained samples was performed using a PANalytical X'Pert Powder diffractometer (Ni-filtered CuKα radiation, PIXcel^{1D} detector, and the exposition corresponded to about 2 s per step of 0.02° over the angular range of 10-100°) at room temperature. *In situ* XRD measurements were conducted in an Anton Paar high-temperature chamber (HTK 16 N) in a temperature range between 300 and 870 K.

To estimate the stability limits of the high-pressure stabilized perovskite phases, the obtained ceramic samples were annealed at temperatures between 870 and 1120 K with a 50 K step followed by XRD study at room temperature after each step. The samples were put in a furnace heated to the certain temperature and quenched in air after a 2-h dwell.

Synchrotron XRD studies were performed at the CRISTAL diffraction beamline by means of micro powder diffraction at high pressure using a Membrane Diamond Anvil Cell (MDAC). Neon was used as a hydrostatic pressure transmitting medium. The diffraction data were collected at room temperature between ambient pressure and 20 GPa upon compression and decompression, using a CCD Rayonix SX165 detector with an exposition time of 2–5 min. Powder diffractorgams were extracted from the images using the Dioptas software suite [26]. The beam energy was 29.8 keV ($\lambda = 0.416$ Å) and the spot size was 40 μm × 40 μm fwhm.

Neutron powder diffraction data were collected at the ISIS pulsed neutron and muon facility of the Rutherford Appleton Laboratory on the WISH diffractometer located at the second target station [27]. The sample was loaded into a cylindrical 3-mm-diameter vanadium can and measured in a temperature range of 1.5–300 K, with the exposition time of 0.5 h using an Oxford Instruments cryostat.

Rietveld refinements of the diffraction data have been performed using FULLPROF package [28] and JANA 2006 software [29].

3. Results and discussion

Based on an analysis of room-temperature neutron and X-ray diffraction patterns of the as-prepared samples (see Fig. S1 of the Supplementary Materials), the compositional ranges of the BL*x*FSO perovskite phases were estimated. In the compositional range of $0 = x \leq 0.05$, the structural phase was identified to be an antipolar *Pnma* one with the $\sqrt{2}a_p \times 4a_p \times 2\sqrt{2}a_p$ superstructure (a_p is the pseudocubic perovskite unit-cell parameter). An incommensurately modulated phase with the *Imma*(00γ)*s*00 superspace group was observed for $0.10 = x \leq 0.33$. The BL*x*FSO compositions with $x \geq 0.34$ were found to crystallize in a non-polar *Pnma* ($\sqrt{2}a_p \times 2a_p \times \sqrt{2}a_p$) structure. No ranges of phase coexistence have been detected.

The same sequence of the structural phases was observed in the $Bi_{1-x}La_xFeO_3$ (BL*x*FO) solid solutions with $x > 0.10$ [21]. BL*x*FO can be formally considered as a section of the $Bi_{1-x}La_xFe_ySc_{1-y}O_3$ system at $y = 0$ (Scheme 1). BL*x*FO is one of the most studied $BiFeO_3$-derived systems, since the entire series can be prepared using the conventional ceramic technique. However, the antipolar *Pnma* ($\sqrt{2}a_p \times 4a_p \times 2\sqrt{2}a_p$) phase observed in $Bi_{0.82}La_{0.18}FeO_3$ was found to exhibit no irreversible structural transitions similar to those detected in the same antipolar phase of $BiFe_{0.5}Sc_{0.5}O_3$ [23]. The main feature of the BL*x*FO series (which is typical of any systems where bismuth is substituted by a rare earth element) is the phase coexistence. Wide ranges of coexistence (in both the compositional scale and the temperature scale) between the antipolar

Pnma ($\sqrt{2}a_p \times 4a_p \times 2\sqrt{2}a_p$) and the non-polar *Pnma* ($\sqrt{2}a_p \times 2a_p \times \sqrt{2}a_p$) phases were reported [8,9,11]. The nature and the content of the coexisting phases are still a matter of discussion.

A phase coexistence is typical for compositions derived from $BiFeO_3$ because their energy landscape consists of several almost degenerated phase states [30]. External impacts, such as pressure applied at the synthesis, can change the balance between those states and make some of them more favourable. The BL*x*FSO phases were synthesized under high pressure followed by a quenching down to room temperature. No transition could occur during the quenching since the kinetics was frozen. Therefore, the structural phases of the as-prepared samples are metastable. This is the main difference of the BL*x*FSO phases from the BL*x*FO ones that were produced at ambient pressure under equilibrium conditions. Moreover, owing to their metastable nature, the high-pressure prepared phases can exhibit the conversion polymorphism phenomenon [31], namely the annealing-stimulated irreversible transitions (provided that the annealing temperature does not exceed the point when metastable phase decomposes into stable (non-perovskite) compositions). The *Pnma* → *R*3*c* → *Ima*2 irreversible transformation in BL0FSO [20] (see *Introduction*) is the prominent example of this phenomenon.

To facilitate a comparative analysis of the structure distortions over the whole compositional range studied, the lattice parameters obtained from the refinements were recalculated into the primitive perovskite unit-cell parameters and angles ($a_p = c_p \neq b_p$, $\alpha_p = \gamma_p = 90^o \neq \beta_p$) using the relations between the basis vectors of the distorted structures and the parent cubic cell reported in Refs. [20,32]. These parameters are closely related to macroscopic strains of the parent perovskite structure and have a clear geometrical meaning. The compositional dependence of the normalized unit cell volume ($V_p = V/Z$, where V is the unit cell volume and Z is the number of the perovskite molecular units per the unit cell) is shown in Fig. 1. The $V_p(x)$ behaviour of BL*x*FSO solid solutions is qualitatively similar to that of the BL*x*FO system [21], although the latter is non-univocal because of the wide compositional ranges of phase coexistence. In both BL*x*FSO and BL*x*FO, the fastest variation of V_p with the lanthanum content is observed in the range between the incommensurately modulated phase with the *Imma*(00γ)*s*00 superspace group and the non-polar orthorhombic *Pnma* phase. In the lanthanum-rich ranges ($x >$ ~0.4), V_p is weakly dependent on x. Non-monotonic behaviour and discontinuity in the compositional variation of the unit cell volume were observed in other perovskite solid solutions with lanthanum-to-bismuth substitutions and attributed to competitions between the electrostatic-type interaction resulted from La^{3+} and the covalent bond associated with a lone-pair configuration of Bi^{3+} [33,34].

Fig. 2 depicts the compositional dependence of the BL*x*FSO primitive perovskite unit cell parameters. One can see that in the range of the antipolar orthorhombic *Pnma* structure ($0 = x \leq 0.05$) the parameters a_p and b_p both decrease with increasing x. In the range of the incommensurately modulated structure derived from *Immm* ($0.10 = x \leq 0.33$), a_p decreases and b_p increases, while when $x \geq 0.34$ (the range of the non-polar *Pnma* structure), the trend changes, namely a_p increases and b_p decreases. It is interesting that in the vicinity of composition with $x = 0.33$ the metric of primitive perovskite unit cell is almost cubic: $a_p \approx b_p$ and $\beta_p \approx 90^o$.

The perovskite ceramics prepared under high pressure were step-by-step annealed as described in *Experimental procedure*. The annealing temperature was increased until the reflections of the cubic sillenite-type $Bi_{19}ScO_{30}$ phase were detected in the XRD patterns [35]. The thermal stability limit was defined as the temperature which is 50 K lower than the temperature at which the sillenite-type phase appears. The stability limit temperature of the BL*x*FSO perovskite phases was found to depend on the lanthanum content and increases with increasing x (Table 1).

Typical microstructure of the high-pressure synthesized BL*x*FSO ceramics is shown in Fig. 3. No regular variation of the microstructure with increase of lanthanum content (which resulted in formation of perovskite phases of a different symmetry) has been observed. The average grain size of the ceramics prepared using a sol-gel combustion route was found to be by a factor of 2–3 smaller than that of the ceramics obtained from a mechanical mixture of the oxides.

As mentioned in *Introduction*, annealing of the as-prepared high-pressure stabilized BL0FSO leads to the irreversible *Pnma* → *R*3*c* → *Ima*2 crossover. An attempt to transform a composition with 5 at.% of lanthanum was unsuccessful: the *Pnma* phase remained up to 970 K. Increasing temperature to 1020 K resulted in decomposition of the orthorhombic BL0.05FSO into the rhombohedral $BiFeO_3$-based phase, $Bi_{19}ScO_{30}$ and some other non-perovskite phases. The temperature dependences of the unit cell parameters of BL0FSO and BL0.05FSO are shown in Fig. 4.

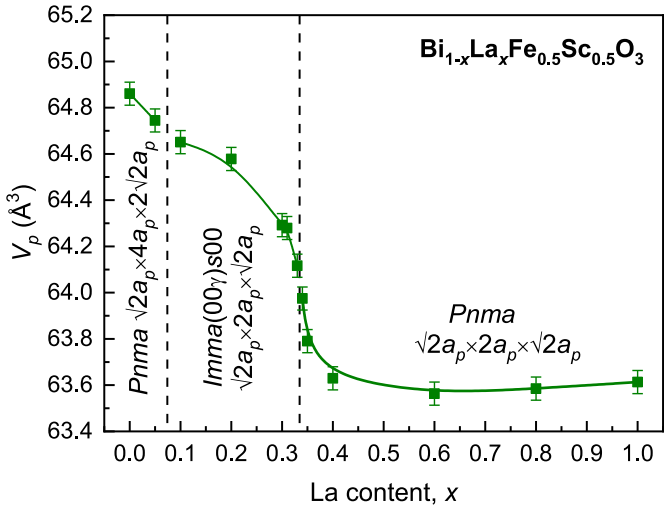

Fig. 1. The normalized unit-cell volume of the BL*x*FSO perovskite phases as a function of the lanthanum content (x) with the tentative borders of the phase ranges. The space groups and the superstructures are indicated (a_p is the pseudocubic primitive perovskite unit-cell parameter).

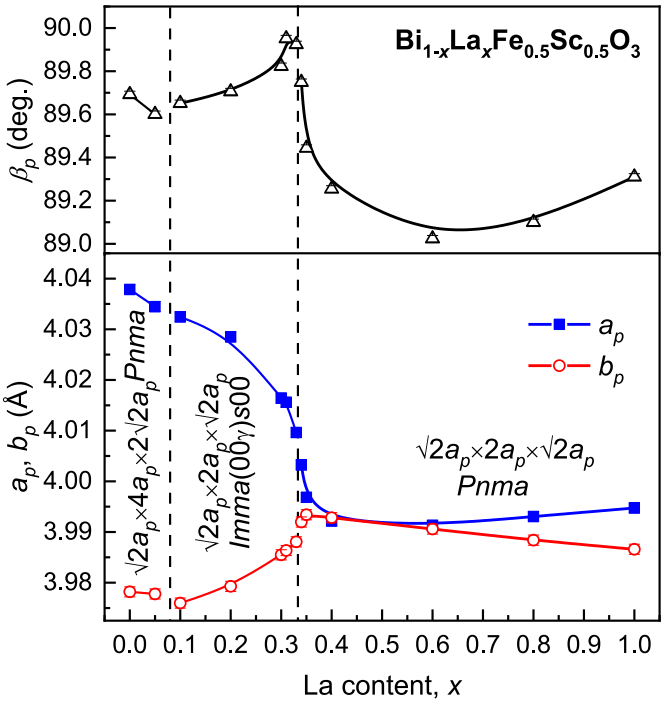

Fig. 2. The primitive perovskite cell parameters of the BL*x*FSO phases as a function of the lanthanum content with the tentative borders of the phase ranges. The space groups and the metric relations are indicated. Error bars are smaller than the symbols.

Table 1
Temperatures of the thermal stability limit of the BL*x*FSO perovskite phases.

Composition	Temperature
$0 = x \leq 0.35$	970 K
$0.35 < x \leq 0.40$	1070 K
$0.40 < x \leq 0.60$	1120 K
$x \geq 0.80$	stable until melting

As seen from Fig. 4, the values of the primitive perovskite cell parameters a_p and b_p of the antipolar orthorhombic *Pnma* phases of BL0FSO and BL0.05FSO as well as their temperature variations are respectively very similar. However, as opposed to BL0FSO, an annealing of BL0.05FSO at temperatures up to its thermal stability limit has resulted in no structural transformation.

The temperature dependences of the normalized unit-cell volume and the primitive perovskite cell angle of both BL0FSO and BL0.05FSO are shown in Figs. S2 and S3 of the Supplementary Materials.

The second and all the next subsequent thermal treatments with maximum temperature of 920 K demonstrated a reversible *Ima*2 ↔ *R*3*c* transition in BL0FSO (Fig. S4) and no transition in BL0.05FSO.

It was revealed from refinement of the XRD patterns of the BL*x*FSO perovskite phases with incommensurate modulation described by the *Imma*(0,0,γ)s00 superspace group ($0.10 = x \leq 0.33$) that the γ value, which is characteristic of the correlated displacements of Bi^{3+} [24] increases with increasing x (Fig. 5). The case of $\gamma = 0.5$ corresponds to the commensurate displacements.

An increase of temperature was found to lead to reversible phase transition (without phase coexistence) in BL*x*FSO with $0.10 = x \leq 0.33$ from the incommensurately modulated phase to the non-polar orthorhombic phase isostructural to $LaFeO_3$ (*Pnma*, $\sqrt{2}a_p \times 2a_p \times \sqrt{2}a_p$) (see Fig. S5 in the Supplementary Materials). Fig. 6 shows the temperature dependences of the unit cell parameters of BL0.10FSO and BL0.32FSO perovskites.

All the BL*x*FSO phases with incommensurate modulation demonstrate the same thermal behaviour of the primitive perovskite cell parameters a_p and b_p at the temperature-induced transition into a non-polar *Pnma* phase, namely $a_p > b_p$ below T_C and $a_p < b_p$ above T_C (Fig. 6).

Temperature dependences of the normalized unit-cell volume and the primitive perovskite cell angles of BL0.10FSO and BL0.32FSO are shown in Figs. S6 and S7.

It was also found from the refinement that the temperature variation of the γ value in the incommensurately modulated BL*x*FSO perovskite phases is constant (0.512 ± 0.002) within the experimental error.

The structural transition temperature expressed as a function of x is shown in Fig. 7.

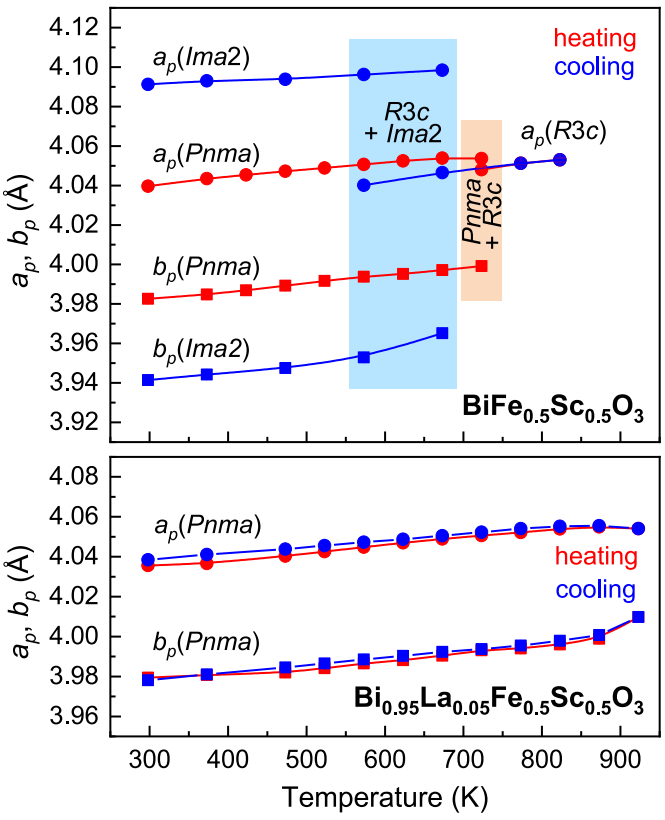

Fig. 4. Temperature dependence of the primitive perovskite cell parameters a_p (solid circles) and b_p (solid squares) of the as-prepared $BiFe_{0.5}Sc_{0.5}O_3$ (top panel) and $Bi_{0.95}La_{0.05}Fe_{0.5}Sc_{0.5}O_3$ (bottom panel) upon annealing. The shadow zones indicate the phase coexistence ranges. Error bars are smaller than the symbols.

It was found from the *in situ* pressure synchrotron XRD study that the incommensurate modulation in BL0.20FSO persists up to 2.9 GPa (see the XRD patterns in Fig. S8). At 2.9 GPa, the *Imma*(00γ)s00 phase of BL0.20FSO transforms into an orthorhombic phase with the same non-polar *Pnma* structure as that observed in this composition at ambient pressure above 700 K. The pressure dependence of the primitive perovskite unit cell parameters of BLa0.20FSO is shown in Fig. 8.

It should be noticed that at the pressure-induced *Imma*(00γ)s00 → *Pnma* transition, the primitive perovskite cell parameters a_p and b_p keep the same ratio, $a_p > b_p$, both below and above T_C.

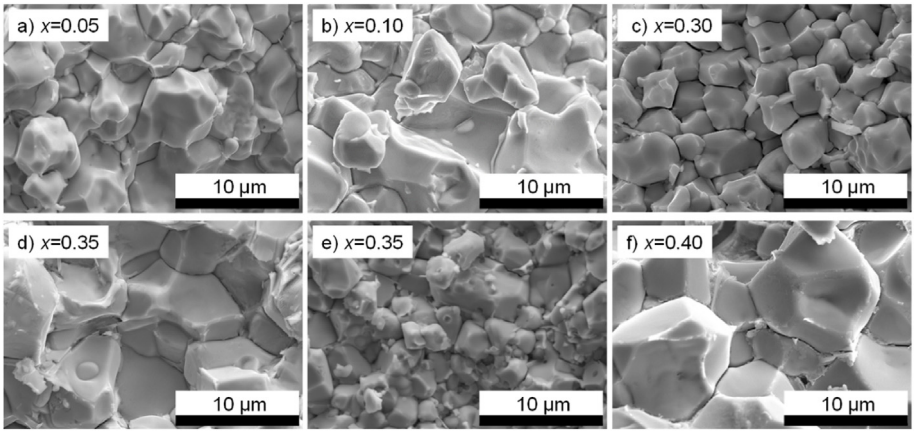

Fig. 3. SEM images of the fractured surfaces of the BL*x*FSO ceramics ($x = 0.05$–0.40) synthesized under high pressure from a mechanical mixture of the respective oxides (a,b,d,f) and from the powders prepared using a sol-gel combustion route (c,e).

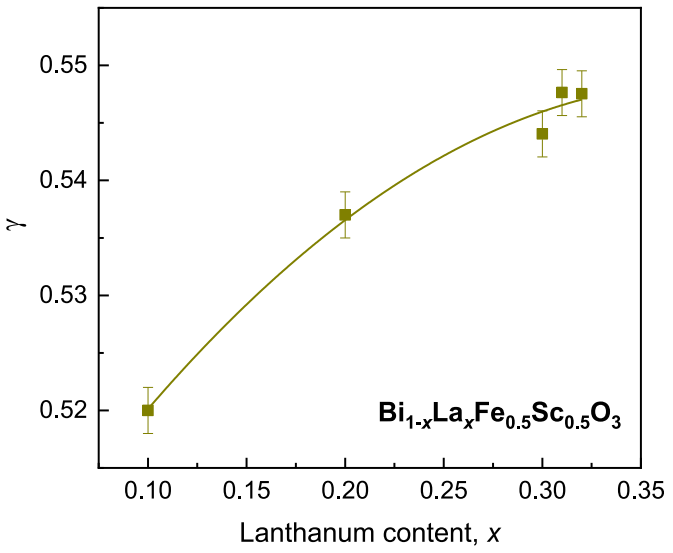

Fig. 5. Compositional dependence of the γ value in the incommensurately modulated BL*x*FSO perovskite phases with the *Imma*(00γ)*s*00 superspace group.

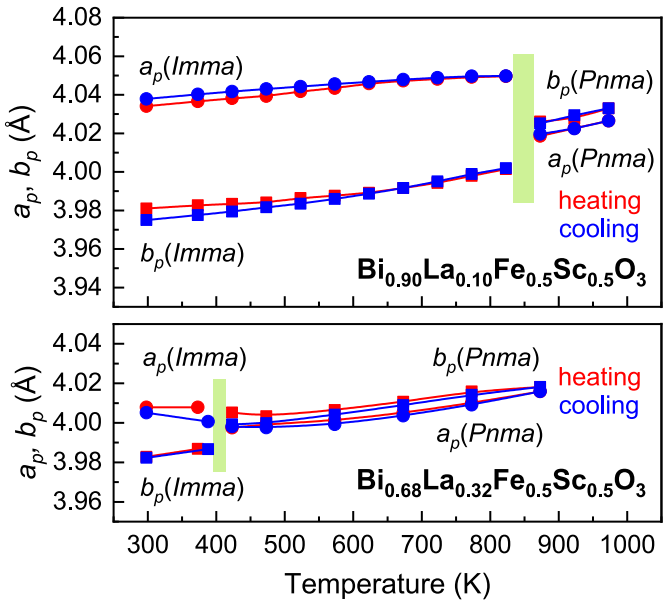

Fig. 6. Temperature dependence of the primitive perovskite cell parameters a_p (solid circles) and b_p (solid squares) of as-prepared $Bi_{0.90}La_{0.10}Fe_{0.5}Sc_{0.5}O_3$ (top panel) and $Bi_{0.68}La_{0.32}Fe_{0.5}Sc_{0.5}O_3$ (bottom panel) upon annealing. The shadow zones indicate the phase transition ranges. Error bars are smaller than the symbols.

Fig. S9 depicts the pressure dependences of the normalized unit-cell volume and the primitive perovskite cell angle of BLa0.20FSO.

The γ value of BL0.20FSO as a function of pressure is shown in Fig. 9. One can see that pressure acts to suppress the incommensurate modulation. At the same time, the structure with incommensurate modulation persists up to the pressure values of a few GPa, until a transformation into the non-polar *Pnma* phase occurs. At this pressure, the γ value is still above 0.5. Such a wide pressure range of stability suggests the possibilities to produce epitaxial films of the metastable perovskite phases with controllable incommensurate modulation on the substrates that would provide a compressive stress.

One can conclude from comparison of the composition- (x), temperature- (T) and pressure- (P) dependent behaviours of the incommensurately modulated BL*x*FSO phases that although the respective dependences of the unit-cell volume and the γ value are different ($\Delta V_p/\Delta x < 0$, $\Delta V_p/\Delta T > 0$ and $\Delta V_p/\Delta P < 0$; $\Delta\gamma/\Delta x > 0$, $\gamma(T) \approx$ const and $\Delta\gamma/\Delta P < 0$), an increase either in the La content, temperature or pressure induces transformation into the non-polar orthorhombic structure accompanied by a negative jump in unit-cell volume.

4. Conclusions

Reversible and irreversible phase transformations between high-pressure stabilized perovskite phases in the entire range of the perovskite $Bi_{1-x}La_xFe_{0.5}Sc_{0.5}O_3$ solid solution system were studied using laboratory and synchrotron X-ray diffraction. The following compositional sequence of structural phases was observed in the as-prepared ceramics at room temperature: an antipolar *Pnma* phase with the $\sqrt{2}a_p \times 4a_p \times 2\sqrt{2}a_p$ superstructure for $x \leq 0.05$, an incommensurately modulated phase with the *Imma*(00γ)*s*00 superspace group for $0.10 = x \leq 0.33$, and a non-polar *Pnma* phase ($\sqrt{2}a_p \times 2a_p \times \sqrt{2}a_p$) for $x \geq 0.34$. No compositional ranges of phase coexistence were detected. The compositional behaviour of the normalized unit-cell volume of the $Bi_{1-x}La_xFe_{0.5}Sc_{0.5}O_3$ perovskites is strongly non-linear in the range of $0 = x \leq 0.60$, which is attributed to competitions between the electrostatic-type interaction resulting from La^{3+} and the covalent bond associated with a lone-pair configuration of Bi^{3+}. The temperature stability limit of the $Bi_{1-x}La_xFe_{0.5}Sc_{0.5}O_3$ perovskite phases at ambient pressure is about 970 K (for a composition with $x = 0$) and slightly increases as the lanthanum content is increased. Compositions with $x \geq 0.8$ can be prepared using the conventional ceramic route. Annealing of the as-prepared samples with composition corresponding to $x = 0$ induces an irreversible structure transformation *Pnma* → *R*3*c* → *Ima*2, while annealing (up to the thermal stability limit) of those with $x = 0.05$ results in no phase transition. In the perovskite solid solutions with $0.10 = x \leq 0.33$, an increase of temperature induces a reversible phase transition from the incommensurately modulated *Imma*(00γ)*s*00 structure to the non-polar orthorhombic *Pnma* one. The transition temperature decreases as the La content is increased. The same type of a reversible transformation, namely *Imma*(00γ)*s*00 → *Pnma* occurs when pressure is increased. The γ value, which characterizes the incommensurate modulation, decreases with increasing pressure but remains above 0.5 until the transition (2.9 GPa in the solid solution with $x = 0.20$).

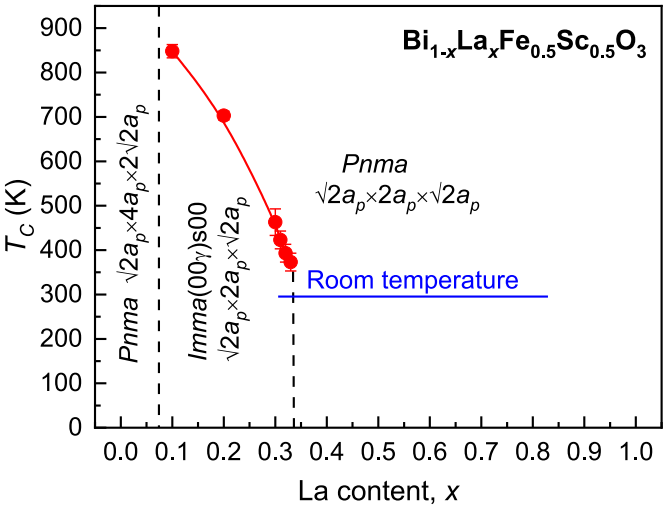

Fig. 7. The transition temperature (T_C) of the of the BLxFSO perovskite phases with the incommensurately modulated structure as a function of the lanthanum content (x) with the tentative borders of the phase ranges.

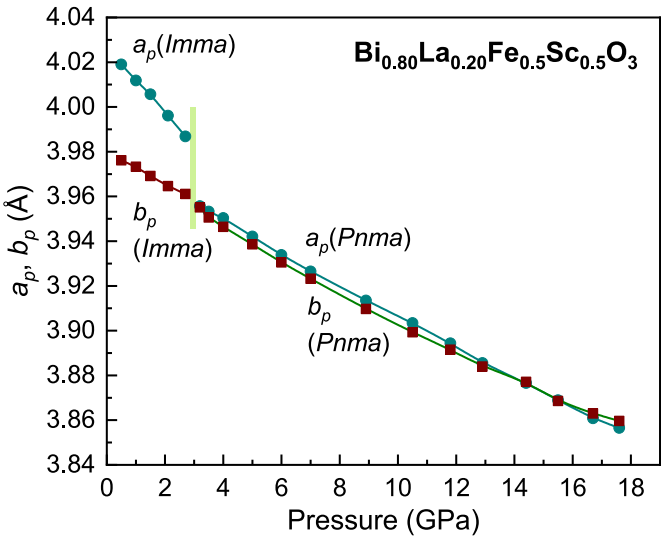

Fig. 8. Pressure dependence of the primitive perovskite cell parameters a_p (solid circles) and b_p (solid squares) of as-prepared $Bi_{0.80}La_{0.20}Fe_{0.5}Sc_{0.5}O_3$ upon compression. The shadow zone indicates the phase transition range. Error bars are smaller than the symbols.

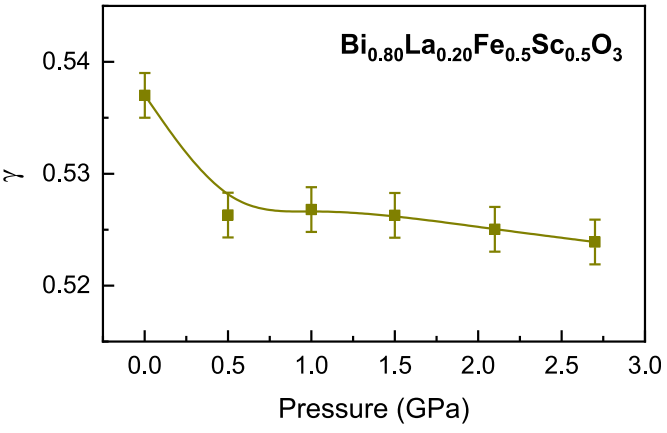

Fig. 9. Pressure dependence of the γ value in the incommensurately modulated as-prepared $Bi_{0.80}La_{0.20}Fe_{0.5}Sc_{0.5}O_3$ phase with the *Imma*(00γ)*s*00 superspace group.

CRediT authorship contribution statement

A.N. Salak: Conceptualization, Methodology, Writing – original draft, Writing – review & editing, Supervision. **J.P. Cardoso:** Investigation, Formal analysis, Data curation, Writing – original draft. **D.D. Khalyavin:** Conceptualization, Investigation, Formal analysis, Writing – review & editing. **A. Barbier:** Validation, Formal analysis, Data curation, Writing – review & editing. **P. Fertey:** Investigation, Data curation, Writing – review & editing. **S.M. Mikhalev:** Methodology, Software, Formal analysis. **N.M. Olekhnovich:** Conceptualization, Methodology, Supervision. **A.V. Pushkarev:** Investigation, Formal analysis, Data curation. **Yu V. Radyush:** Investigation, Formal analysis, Data curation, Visualization. **A. Stanulis:** Investigation, Formal analysis, Data curation. **R. Ramanauskas:** Conceptualization, Methodology.

Declaration of competing interest

The authors declare that they have no known competing financial interests or personal relationships that could have appeared to influence the work reported in this paper.

Data availability

Data will be made available on request.

Acknowledgements

J.P.C. is grateful to FCT – the Portuguese Foundation for Science and Technology for the financial support through the individual PhD grant SFRH/BD/145281/2019. A.N.S. and S.M.M. acknowledge the financial support of national funds (OE) through FCT in the scope of the framework contract foreseen in the numbers 4, 5, and 6 of the article 23, of the Decree-Law 57/2016, of August 29, changed by Law 57/2017, of July 19. The research done in the University of Aveiro was supported by the project CICECO-Aveiro Institute of Materials, UIDB/50011/2020, UIDP/50011/2020 & LA/P/0006/2020, financed by national funds through the FCT/MCTES (PIDDAC). The authors also acknowledge SOLEIL for provision of synchrotron radiation at the CRISTAL beamline in frame of the experiment No 20210529. KNMF at the Karlsruhe Institute of Technology is also acknowledged for the provision of the SU-8 compound refractive lenses focusing optic at the CRISTAL beamline.

Appendix A. Supplementary data

Supplementary data to this article can be found online at https://doi.org/10.1016/j.jssc.2023.123937.

References

[1] G. Catalan, J.F. Scott, Physics and applications of bismuth ferrite, Adv. Mater. 21 (2009) 2463–2485.
[2] A.P. Pyatakov, A.K. Zvezdin, Magnetoelectric and multiferroic media, Phys. Usp. 55 (6) (2012) 557–581.
[3] J. Wua, Z. Fan, D. Xiao, J. Zhu, J. Wang, Multiferroic bismuth ferrite-based materials for multifunctional applications: ceramic bulks, thin films and nanostructures, Prog. Mater. Sci. 84 (2016) 335–402.
[4] B. Deka, K.H. Cho, $BiFeO_3$-based relaxor ferroelectrics for energy storage: progress and prospects, Materials 14 (2021) 7188.
[5] N. Wang, X. Luo, L. Han, Z. Zhang, R. Zhan, H. Olin, Y. Yang, Structure, performance, and application of $BiFeO_3$ nanomaterials, Nano-Micro Lett. 12 (2020) 81.
[6] I. Sosnowska, T. Peterlin-Neumaier, E. Steichele, Spiral magnetic ordering in bismuth ferrite, J. Phys. C Solid State Phys. 15 (1982) 4835–4846.
[7] K.P. Andryushin, V.P. Sakhnenko, A.V. Turik, L.A. Shilkina, A.A. Pavelko, S.I. Dudkina, A.G. Rudskaya, D.D. Rudskiy, I.A. Verbenko, S.V. Hasbulatov, L.A. Reznichenko, I.A. Parinov, S.H. Chang, H.Y. Wang, Reasons for the high electrical conductivity of bismuth ferrite and ways to minimize it, Appl. Sci. 11 (2021) 1025.
[8] C.H. Yang, D. Kan, I. Takeuchi, V. Nagarajan, J. Seidel, Doping $BiFeO_3$: approaches and enhanced functionality, Phys. Chem. Chem. Phys. 14 (2012) 15953–15962.
[9] D.C. Arnold, Composition-driven structural phase transitions in rare-earth-doped $BiFeO_3$ ceramics: a review, IEEE Trans. Ultrason. Ferroelectrics Freq. Control 62 (2015) 62–82.
[10] J. Gebhardt, A.M. Rappe, Doping of $BiFeO_3$: a comprehensive study on substitutional doping, Phys. Rev. B 98 (2018), 125202.
[11] F. Mumtaza, S. Nasira, G. Hassnain Jaffaria, S. Ismat Shah, Chemical pressure exerted by rare earth substitution in $BiFeO_3$: effect on crystal symmetry, band structure and magnetism, J. Alloys Compd. 876 (2021), 160178.
[12] M. Azuma, H. Kanda, A.A. Belik, Y. Shimakawa, M. Takano, Magnetic and structural properties of $BiFe_{1-x}Mn_xO_3$, J. Magn. Magn Mater. 310 (2007) 1177–1179.
[13] K. Oka, T. Koyama, T. Ozaaki, S. Mori, Y. Shimakawa, M. Azuma, Polarization rotation in the monoclinic perovskite $BiCo_{1-x}Fe_xO_3$, Angew. Chem. Int. Ed. 51 (2012) 7977–7980.
[14] A.A. Belik, D.A. Rusakov, T. Furubayashi, E. Takayama-Muromachi, $BiGaO_3$-based perovskites: a large family of polar materials, Chem. Mater. 24 (2012) 3056–3064.
[15] Z. Pan, J. Chen, R. Yu, H. Yamamoto, Y. Rong, L. Hu, Q. Li, K. Lin, L. You, K. Zhao, L. Fan, Y. Ren, K. Kato, M. Azuma, X. Xing, Giant polarization and high temperature monoclinic phase in a lead-free perovskite of $Bi(Zn_{0.5}Ti_{0.5})O_3$-$BiFeO_3$, Inorg. Chem. 55 (2016) 9513–9516.
[16] I.P. Raevski, S.P. Kubrin, A.V. Pushkarev, N.M. Olekhnovich, Y.V. Radyush, V.V. Titov, M.A. Malitskaya, S.I. Raevskaya, H. Chen, The effect of Cr substitution for Fe on the structure and magnetic properties of $BiFeO_3$ multiferroic, Ferroelectrics 525 (2018) 1–10.
[17] V.S. Rusakov, V.S. Pokatilov, A.S. Sigov, A.A. Belik, M.E. Matsnev, Changes in the magnetic structure of multiferroic $BiFe_{0.80}Cr_{0.20}O_3$ with temperature, Phys. Solid State 61 (2019) 1030–1036.
[18] A.N. Salak, J.P.V. Cardoso, J.M. Vieira, V.V. Shvartsman, D.D. Khalyavin, E.L. Fertman, A.V. Fedorchenko, A.V. Pushkarev, Y.V. Radyush, N.M. Olekhnovich,

R. Tarasenko, A. Feher, E. Čižmár, Magnetic behaviour of perovskite compositions derived from $BiFeO_3$, Magnetochemistry 7 (11) (2021) 151.

[19] J. Kaczkowski, M. Pugaczowa-Michalska, I. Płowas-Korus, Comparative density functional studies of pristine and doped bismuth ferrite polymorphs by GGA+*U* and *meta*-GGA SCAN+*U*, Phys. Chem. Chem. Phys. 23 (2021) 8571–8584.

[20] D.D. Khalyavin, A.N. Salak, N.M. Olekhnovich, A.V. Pushkarev, Y.V. Radyush, P. Manuel, I.P. Raevski, M.L. Zheludkevich, M.G.S. Ferreira, Polar and antipolar polymorphs of metastable perovskite $BiFe_{0.5}Sc_{0.5}O_3$, Phys. Rev. B 89 (2014), 174414.

[21] D.A. Rusakov, A.M. Abakumov, K. Yamaura, A.A. Belik, G. Van Tendeloo, E. Takayama-Muromachi, Structural evolution of the $BiFeO_3$-$LaFeO_3$ system, Chem. Mater. 23 (2011) 285–292.

[22] A.N. Salak, D.D. Khalyavin, I. Zamaraite, A. Stanulis, A. Kareiva, A.D. Shilin, V.V. Rubanik, Y.V. Radyush, A.V. Pushkarev, N.M. Olekhnovich, M. Starykevich, R. Grigalaitis, M. Ivanov, J. Banys, Metastable perovskite $Bi_{1-x}La_xFe_{0.5}Sc_{0.5}O_3$ phases in the range of the compositional crossover, Phase Transitions 90 (9) (2017) 831–839.

[23] V.V. Shvartsman, D.D. Khalyavin, N.M. Olekhnovich, A.V. Pushkarev, Y.V. Radyush, A.N. Salak, Spontaneous and induced ferroelectricity in the $BiFe_{1-x}Sc_xO_3$ perovskite ceramics, Phys. Status Solidi A 218 (19) (2021), 2100173.

[24] D.D. Khalyavin, A.N. Salak, A.B. Lopes, N.M. Olekhnovich, A.V. Pushkarev, Y.V. Radyush, E.L. Fertman, V.A. Desnenko, A.V. Fedorchenko, P. Manuel, A. Feher, J.M. Vieira, M.G.S. Ferreira, Magnetic structure of an incommensurate phase of La-doped $BiFe_{0.5}Sc_{0.5}O_3$: role of antisymmetric exchange interactions, Phys. Rev. B 92 (2015), 224428.

[25] D.D. Khalyavin, A.N. Salak, P. Manuel, N.M. Olekhnovich, A.V. Pushkarev, Y.V. Radysh, A. Fedorchenko, E.L. Fertman, V.A. Desnenko, M.G.S. Ferreira, Antisymmetric exchange in La-substituted $BiFe_{0.5}Sc_{0.5}O_3$ system: symmetry adapted distortion modes approach, Z. für Kristallogr. - Cryst. Mater. 230 (2015) 767–774.

[26] C. Prescher, V.B. Prakapenka, DIOPTAS: a program for reduction of two-dimensional X-ray diffraction data and data exploration, High Pres. Res. 35 (2015) 223–230.

[27] L.C. Chapon, P. Manuel, P.G. Radaelli, C. Benson, L. Perrott, S. Ansell, N.J. Rhodes, D. Raspino, D. Duxbury, E. Spill, J. Norris, Wish: the new powder and single crystal magnetic diffractometer on the second target station, Neutron News 22 (2011) 22–25.

[28] J. Rodriguez Carvajal, Recent advances in magnetic structure determination by neutron powder diffraction, Phys. B Condens. Matter 192 (1993) 55–69.

[29] V. Petříček, M. Dušek, L. Palatinus, Crystallographic computing system JANA2006: general features, Z. für Kristallogr. - Cryst. Mater. 229 (2014) 345–352.

[30] A. Singh, V.N. Singh, E. Canadell, J. Iniguez, O. Dieguez, Polymorphism in Bi-based perovskite oxides: a first-principles study, Phys. Rev. Mater. 2 (2018), 104417.

[31] D.D. Khalyavin, A.N. Salak, E.L. Fertman, O.V. Kotlyar, E. Eardley, N.M. Olekhnovich, A.V. Pushkarev, Y.V. Radyush, A.V. Fedorchenko, V.A. Desnenko, P. Manuel, L. Ding, E. Čižmár, A. Feher, The phenomenon of conversion polymorphism in Bi-containing metastable perovskites, Chem 55 (32) (2019) 4683–4686.

[32] A.N. Salak, D.D. Khalyavin, P.Q. Mantas, A.M.R. Senos, V.M. Ferreira, Structure-dependent microwave dielectric properties of (1-*x*)$La(Mg_{1/2}Ti_{1/2})O_3$–*x*$La_{2/3}TiO_3$ ceramics, J. Appl. Phys. 98 (2005), 034101.

[33] A.N. Salak, V.M. Ferreira, Structure and dielectric properties of the (1-*x*)$La(Mg_{1/2}Ti_{1/2})O_3$ – *x*$(Na_{1/2}Bi_{1/2})TiO_3$ microwave ceramics, J. Phys. Condens. Matter 18 (2006) 5703–5713.

[34] A.N. Salak, V.M. Ferreira, J.L. Ribeiro, L.G. Vieira, R.C. Pullar, N.McN. Alford, Bismuth-induced dielectric relaxation in the (1-*x*)$La(Mg_{1/2}Ti_{1/2})O_3$ – *x*$Bi(Mg_{1/2}Ti_{1/2})O_3$ perovskite system, J. Appl. Phys. 104 (2008), 014105.

[35] A.N. Salak, D.D. Khalyavin, A.V. Pushkarev, YuV. Radyush, N.M. Olekhnovich, A.D. Shilin, V.V. Rubanik, Phase formation in the (1-*y*)$BiFeO_3$-*y*$BiScO_3$ system under ambient and high pressure, J. Solid State Chem. 247 (2017) 90–96.